

Semi-supervised Segmentation via Uncertainty Rectified Pyramid Consistency and Its Application to Gross Target Volume of Nasopharyngeal Carcinoma

Xiangde Luo¹, Wenjun Liao², Jieneng Chen³, Tao Song⁴, Yinan Chen^{4,5}, Guotai Wang^{1*}, and Shaoting Zhang^{1,4}

¹School of Mechanical and Electrical Engineering, University of Electronic Science and Technology of China, Chengdu, Chengdu, China

²West China Hospital, Sichuan University, Chengdu, China

³College of Electronics and Information Technology, Tongji University, Shanghai, China

⁴SenseTime Research, Shanghai, China

⁵West China Hospital-SenseTime Joint Lab, West China Biomedical Big Data Center, Sichuan University West China Hospital, Chengdu, China

Abstract. Gross Target Volume (GTV) segmentation plays an irreplaceable role in radiotherapy planning for Nasopharyngeal Carcinoma (NPC). Despite that convolutional neural networks (CNN) have achieved good performance for this task, they rely on a large set of labeled images for training, which is expensive and time-consuming to acquire. Recently, semi-supervised methods that learn from a small set of labeled images with a large set of unlabeled images have shown potential for dealing with this problem, but it is still challenging to train a high-performance model with the limited number of labeled data. In this paper, we propose a novel framework with Uncertainty Rectified Pyramid Consistency (URPC) regularization for semi-supervised NPC GTV segmentation. Concretely, we extend a backbone segmentation network to produce pyramid predictions at different scales, the pyramid predictions network (PPNet) was supervised by the ground truth of labeled images and a multi-scale consistency loss for unlabeled images, motivated by the fact that prediction at different scales for the same input should be similar and consistent. However, due to the different resolution of these predictions, encouraging them to be consistent at each pixel directly is not robust and may bring much noise and lead to performance drop. To deal with this dilemma, we further design a novel uncertainty rectifying module to enable the framework to gradually learn from meaningful and reliable consensual regions at different scales. Extensive experiments on our collected NPC dataset with 258 volumes show that our method can largely improve performance by incorporating the unlabeled data, and this framework achieves a promising result compared with existing semi-supervised methods, which achieves 81.22% of mean *DSC* and 1.88 voxels of mean *ASD* on the test set, where only 20% of the training set were annotated. Code is online available: <https://github.com/HiLab-git/SSL4MIS>.

Keywords: Semi-supervised learning · Uncertainty rectifying · Pyramid consistency · Gross Target Volume · Nasopharyngeal Carcinoma

* Corresponding author: guotai.wang@uestc.edu.cn

1 Introduction

Nasopharyngeal Carcinoma (NPC) is one of the most common cancers in southern China, Southeast Asia, the Middle East, and North Africa [5]. The mainstream treatment strategy for NPC is radiotherapy, thus the accurate target delineation plays an irreplaceable factor for precise and effective radiotherapy. However, manual nasopharyngeal tumor contouring is tedious and laborious, since both the nasopharynx gross tumor volume (GTVnx) and lymph node gross tumor volume (GTVnd) need to be accurately delineated from 3D volumetric data [13]. In addition, due to nasopharyngeal tumors have a complex structure, anatomical location and variable invasiveness property, the radiologists have to go through all slices to check the delineation. Even doing this, there are certain local failures caused by delineation missing [13]. Recently, with a large amount of labeled data, deep learning has shown the potential for accurate GTV segmentation [13]. However, collecting a large labeled dataset for network training is hard, as both time and domain knowledge are needed to produce accurate annotation. In contrast, collecting a large set of unlabeled data is easier, which inspired us to develop a semi-supervised approach for NPC GTV segmentation by leveraging unlabeled data. What's more, semi-supervised learning (SSL) can largely reduce the workload of annotators for the development of deep learning models.

Recently, in the medical image computing community, SSL has been widely used for medical image computing to reduce the annotation efforts [9, 12, 16, 19]. Bai et al [1] developed an iterative framework where in each iteration, pseudo labels for unannotated images are predicted by the network and refined by a Conditional Random Field (CRF), then the new pseudo labels are used to update the network. After that, the perturbations-based methods have achieved increasing attentions in semi-supervised medical image segmentation [2, 4, 12, 19], these methods perform the semi-supervised fashion by adding small perturbations to the unlabeled samples and enforce the consistency between the model predictions on the original data and the perturbed data. Meanwhile, the mean teacher-based [21] self-ensembling methods [7, 9, 26, 28] were introduced for semi-supervised medical image segmentation. Following [7], some recent works [9, 26, 28] used the uncertainty to guide the student model to learn more stably. Cao et al. [3] extended the temporal-ensembling model [10] with the uncertainty guidance for mass segmentation from automated breast ultrasound images. Co-training [20] with uncertainty guidance [27] and deep multi-planar training [32] were also introduced for semi-supervised 3D medical image segmentation. In [11, 17, 30], an adversarial training strategy was used as regularization for SSL, which aims to minimize the adversarial loss to encourage the prediction of unlabeled data is anatomical plausible. Luo et al. [15] propose a dual-task consistency framework for SSL by minimizing the difference between the pixel-wise classification and level set regression. The common limitations of these methods are that they just consider the data/task-level perturbations and ignore the prediction discrepancy of different scales in a single model and most of them require much computational cost as they need to perform forward pass many times in an iteration.

In this work, we propose a novel semi-supervised learning framework for the segmentation of GTVnx and GTVnd by further utilizing the unlabeled data. Our method leverages a network that gives a pyramid (i.e., multi-scale) prediction, and encourages

the prediction at multiple scales to be consistent for the same input, which is a simple yet efficient idea for SSL. A standard supervised loss at multiple scales is used for learning from labeled images. For unlabeled images, we encourage the multi-scale predictions to be consistent, which serves as regularization. Since the ground truth of unlabeled images are unknown, the model may produce some unreliable prediction or noise which may cause the model to collapse or over-fit. To overcome these problems, some existing works [3, 28] have introduced the model uncertainty to boost the stability of training and obtain better results. However, they typically estimate the uncertainty of each target prediction with Monte Carlo sampling [8], which needs massive computational costs as it requires multiple forward passes to obtain the uncertainty in each iteration. Differently from these methods, we estimate the uncertainty via the prediction discrepancy among multi-scale predictions, which just needs a single forward pass. With the guidance of the estimated uncertainty, we automatically emphasize the reliable predictions (low uncertainty) and weaken the unreliable ones (high uncertainty) when calculating the multi-scale consistency. Meanwhile, we introduce the uncertainty minimization [31] to reduce the prediction variance during training. Therefore, the Uncertainty Rectified Pyramid Consistency (URPC) framework could be optimized with more reliable supervision by taking advantage of the unlabeled images. The major contributions of this work are summarized as follows:

- We present a novel single-model based semi-supervised learning framework, where a pyramid consistency regularization is proposed to effectively leverage the unlabeled data by minimizing the prediction discrepancy.
- We introduce a novel single forward pass-based uncertainty estimation method and further integrate it into the pyramid consistency framework to more reliably learn from unlabeled data.
- We perform an extensive set of experiments on a clinical-relevant dataset and compare the proposed method against five existing approaches. Results show our URPC largely improves the supervised method performance by utilizing the unlabeled data and also outperforms other existing semi-supervised learning methods.

2 Methods

The overall of the proposed URPC for semi-supervised segmentation is illustrated in Fig. 1. We use a network (i.e., PPNet) that gives a pyramid prediction of the segmentation. PPNet learns from the labeled data by minimizing the supervised loss directly. In addition, the PPNet is regularized by a multi-scale consistency between the pyramid predictions to deal with unlabeled data. The PPNet naturally leads to an uncertainty by measuring the discrepancy between these predictions, and we propose to use this uncertainty to rectify the pyramid consistency considering the different spatial resolutions in the pyramid. To describe this work precisely, we firstly define some mathematical terms. Let \mathcal{D}_l , \mathcal{D}_u and $f_\phi(x)$ be the labeled set, unlabeled set and the given network, respectively. Let $\mathcal{D} = \mathcal{D}_l \cup \mathcal{D}_u$ be the whole provided dataset. We denote labeled data pair as $(x_i, y_i) \in \mathcal{D}_l$ and unlabeled data as $x_i \in \mathcal{D}_u$, where y_i is ground truth.

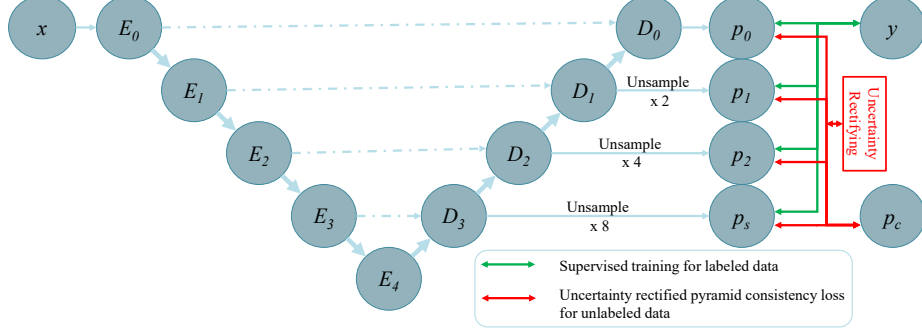


Fig. 1. Overview of the proposed novel URPC, which consists of a pyramid predictions network (PPNet) and an uncertainty rectifying module. The URPC is optimized by minimizing the supervised loss on the labeled data and the pyramid consistency loss on the unlabeled data. In addition, an uncertainty rectifying module is designed to reduce the impact of noise in the pyramid consistency and boost the stability of training.

2.1 Multi-Scale Prediction Network with Pyramid Consistency

To better exploit the prediction discrepancy of a single model at different scales, we firstly introduce the pyramid prediction network (PPNet) to perform segmentation task, which can produce predictions with different scales. In this work, we employ 3D UNet [6] as our framework backbones, and we modify the 3D UNet to produce the pyramid prediction by adding a classification layer after each upsample block in the decoder. To introduce more perturbations in the network, the dropout and feature-level noise layers were added before these classification layers. For an input image x , the given network $f_\phi(x)$ produces a set of multi-scale predictions $[p'_0, p'_1, \dots, p'_s, \dots, p'_{S-1}]$, where the p'_s is the prediction at s th scale, and S is total number of scales. Then, we rescale these multi-scale predictions to the input size, and the corresponding results are denoted as $[p_0, p_1, \dots, p_s, \dots, p_{S-1}]$. For the labeled data, we use a supervised loss that is a combination of Dice and cross-entropy loss at multiple scales:

$$\mathcal{L}_{sup} = \frac{1}{S} \sum_{i=0}^{S-1} \frac{\mathcal{L}_{dice}(p_i, y) + \mathcal{L}_{ce}(p_i, y)}{2} \quad (1)$$

where y , \mathcal{L}_{dice} , \mathcal{L}_{ce} denote the ground truth of input x , the Dice loss and the cross entropy loss, respectively.

To efficiently leverage unlabeled data for training, we introduce a regularization by encouraging the multi-scale predictions of the PPNet be consistent. Concretely, we design a pyramid consistency loss to minimize the discrepancy (i.e., variance) among the predictions at different scales. First, we denote the average prediction across these scales as:

$$p_c = \frac{1}{S} \sum_{i=0}^{S-1} p_i \quad (2)$$

Then, the pyramid consistency loss is defined as:

$$\mathcal{L}_{pyc} = \frac{1}{S} \sum_{i=0}^{S-1} \|p_i - p_c\|^2 \quad (3)$$

where we encourage a minimized *L2* distance between the prediction at each scale and the average prediction.

2.2 Uncertainty Rectified Pyramid Consistency Loss

As the pyramid prediction at a range of scales have different spatial resolutions, even they can be resampled to the same resolution as the input, the resampled results still have different spatial frequencies, i.e., the prediction at the lowest resolution captures the low-frequency component of the segmentation, and the prediction at the highest resolution obtains more high-frequency components. Directly imposing a voxel-level consistency among these predictions can be problematic due to the different frequencies. Inspired by existing works [3, 24, 25, 28, 31], we introduce an uncertainty-aware method to address these problems. Different from these methods, this method estimate uncertainty is a scale-level approach and only with a single forward pass, which needs less computational cost and running time than exiting methods.

Uncertainty Estimation. In this work, inspired by these fast uncertainty estimation approaches [24, 31], we model the scale-level uncertainty via the prediction variance between the average prediction and each scale output. To be specific, we use the KL-divergence between the average prediction and the *i*th prediction as the *i*th scale variance:

$$\mathcal{D}_i = \sum_{j=0}^C p_i^j \cdot \log \frac{p_i^j}{p_c^j} \quad (4)$$

where the *j* means the *j*th class, and *C* is the total number of the class of prediction. The approximated variance shows the difference between the p_i and p_c if the value is large means two predictions are not similar. It reflects the uncertainty of the model at the *i*th scale prediction. It is worthy to note that the uncertainty is voxel-wise and has the same shape as the input image.

Uncertainty Rectifying. Based on the estimated the variance map \mathcal{D}_i , we further extend the pyramid consistency \mathcal{L}_{pyc} to emphasize reliable prediction and ignore unreliable prediction for stable unsupervised training. Specifically, for unlabeled data, we use the estimated uncertainty map to automatically select reliable voxels for network parameters update. The rectified pyramid consistency loss is formulated as:

$$\mathcal{L}_{unsup} = \underbrace{\frac{1}{S} \frac{\sum_{i=0}^{S-1} \|p_i - p_c\|^2 \cdot w_i}{\sum_{i=0}^{S-1} w_i}}_{uncertainty rectification} + \underbrace{\frac{1}{S} \sum_{i=0}^{S-1} \mathcal{D}_i}_{uncertainty minimization} \quad (5)$$

where the consistency loss consists of two terms, the first is an uncertainty rectification (UR) term and the second is uncertainty minimization (UM) term. For a more stable training, we follow the policy in [31] that we use the voxel-wise weighted w to automatically rectify the MSE loss rather than the threshold-based cut off approaches [3,28], as the threshold is hard to determine. The w_i^v is defined as:

$$w_i^v = e^{-\mathcal{D}_i^v} \quad (6)$$

where the v means the v *th* voxel in the image. According to this definition, the higher uncertainty leads to lower weight automatically. In addition, to encourage the PPNet to produce more consistent predictions at different scales, we use the uncertainty minimization term as a constraint directly. With this uncertainty rectified consistency loss, the PPNet can learn more reliable knowledge, which can then reduce the overall uncertainty of the model and produce more consistent predictions.

2.3 The Overall Loss Function

The proposed URPC framework learns from both labeled data and unlabeled data by minimizing the following combined objective function:

$$\mathcal{L}_{total} = \mathcal{L}_{sup} + \lambda \cdot \mathcal{L}_{unsup} \quad (7)$$

where \mathcal{L}_{sup} , \mathcal{L}_{unsup} are defined in Eq. 1 and Eq. 3, respectively. λ is a widely-used time-dependent Gaussian warming up function [21, 28] to control the balance between the supervised loss and unsupervised consistency loss, which is defined as:

$$\lambda(t) = w_{max} \cdot e^{(-5(1 - \frac{t}{t_{max}})^2)} \quad (8)$$

where w_{max} means the final regularization weight, t denotes the current training step and t_{max} is the maximal training step.

3 Experiments and Results

3.1 Dataset and metrics

The NPC dataset. The NPC dataset used in this work was collected from the West China Hospital, Sichuan University. A total number of 258 T1-weighted MRI cases (from 258 patients) of NPC were acquired on several 3T Siemens scanners. The mean resolution of this dataset is $1.23mm \times 1.23mm \times 1.10mm$ and the mean dimension is $176 \times 286 \times 245$. The ground truth for GTVnx and GTVvd were obtained from manual segmentation by two experienced radiologists using ITK-SNAP [29], and confirmed by an independent senior expert. The dataset was randomly split into 180 cases for training, 20 cases for validation, and 58 cases for testing. For preprocessing, we normalize each scan to zero mean and unit variance.

Table 1. Ablation study of the proposed URPC framework on the NPC MRI dataset, where using 10% labeled data for training. UR and UM denote the uncertainty rectification term and uncertainty minimization term, respectively.

Method	GTVnx		GTVnd		Mean	
	DSC (%)	ASD (voxel)	DSC (%)	ASD (voxel)	DSC (%)	ASD (voxel)
Baseline (S = 1)	71.94	2.42	66.27	3.60	69.10	3.01
S = 2	79.88	1.79	72.82	2.85	76.35	2.32
S = 3	79.09	1.76	75.08	2.25	77.09	2.05
S = 4	80.13	1.82	75.83	2.65	77.98	2.24
S = 5	79.10	1.84	75.73	2.29	77.42	2.06
S = 4 with UR	80.99	1.70	75.22	3.05	78.11	2.38
S = 4 with UR and RM	80.76	1.69	75.95	2.20	78.36	1.95

Evaluation Metrics Following existing work [13], we used the commonly-adopted Dice Similarity Coefficient (*DSC*) and the Average Surface Distance (*ASD*) as segmentation quality evaluation metrics. For a fair comparison, we reported the mean *DSC* and *ASD* of different methods on the testing set, and all of them without using any post-processing strategy.

3.2 Implementations

The framework was implemented in PyTorch [18], using a node of a cluster with 8 TiTAN 1080TI GPUs. We used the SGD optimizer (weight decay=0.0001, momentum=0.9) with a joint cross-entropy loss and dice loss [28] to update the network parameters. During the training processing, the poly learning rate strategy was used for learning rate decay, where the initial learning rate is multiplied by $(1.0 - \frac{iter}{max_iter})^{power}$ with a *power* 0.9 and the initial learning rate and the *max_iter* were set to 0.1 and 60k. The batch size was set to 4 for the NPC dataset, due to the limited GPU memory. Each batch consists of two annotated images and two unannotated images. During the training stage, We randomly cropped $112 \times 112 \times 112$ sub-volumes as the network input and employed conventional data augmentation to enlarge dataset and avoid over-fitting, including random crop, random flip and random rotate. During the inference stage, a sliding window strategy with a stride of $64 \times 64 \times 64$ was used to obtain the final segmentation results. For a fair comparison with the state-of-the-art methods, we used the open-source implementations [14] of them for all experiments and reported the results. The hyper-parameter of the weight factor (λ) of the unsupervised loss was set to $w_{max} = 0.1$ for all experiments.

3.3 Evaluation of Our Proposed SSL Approach on the NPC dataset

Ablation Study on the NPC dataset. Firstly, to investigate the impact of different numbers of scale outputs for PPNet, as shown in Fig. 1, we compared the baseline with PPNet where the *S* was set to 2, 3, 4, and 5, respectively. In this study, the baseline is the 3D UNet without multi-scale predictions and therefore it only learns from labeled data. In contrast, the variants of PPNet learn from labeled data and the PPNet learns

from both labeled data and unlabeled data. Secondly, to measure the contribution of the uncertainty rectifying module, we performed an ablation study where we add each term of the uncertainty rectifying module (UR term and UM term) into the $S=4$ increasingly. We carried out these study on the NPC dataset with only 10% scans labeled (18 labeled scans and 162 unlabeled scans). The quantitative the results are shown in Tab. 1. It can be found that when the S increases from 2 to 4, the performance of the proposed URPC improves gradually. However, we found that $S = 5$ achieved a lower performance than $S = 4$. This is mainly because that the resolution of of p_4 is too small, and it is 16 times lower than p_0 . Therefore, we used $S = 4$ for SSL in the following experiments. From Tab. 1, we can see that both uncertainty rectifying (UR) term and uncertainty minimization (UM) term boost the model performance. What's more, combining all sub-modules into a unified framework results in a better gain where the mean *DSC* and *ASD* were improved by 9.26% and 1.06 respectively, demonstrating their effectiveness for semi-supervised segmentation.

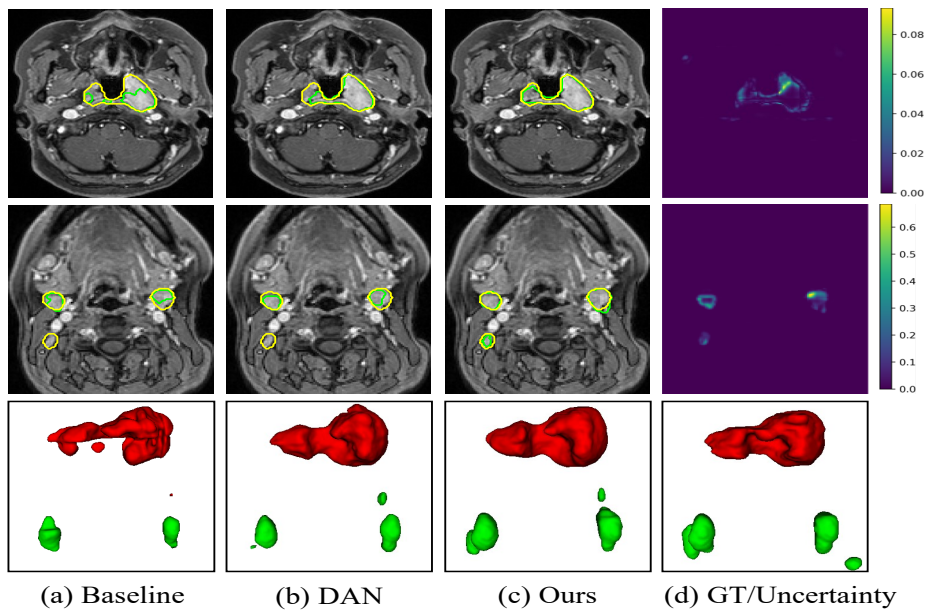


Fig. 2. Visualization of the results by different methods and uncertainty map obtained by our method. The results are based on 10% labeled data and 90% unlabeled data. Lime and yellow contours denote the prediction and ground truth, respectively. In 3D results, the red and green colors show the GTVnx and GTVnd segmentation, respectively.

Comparison with Other Semi-supervised Methods. We compared our method against only using the annotated images for supervised learning with 3D UNet, which is denoted as SL. In addition, we compared several state-of-the-art semi-supervised segmen-

Table 2. Comparison between our method and existing methods on the NPC MRI dataset.

Labeled %	Method	GTVnx		GTVnd		Mean		FT
		DSC (%)	ASD (voxel)	DSC (%)	ASD (voxel)	DSC (%)	ASD (voxel)	
10%	SL	83.93	1.35	83.10	1.48	83.51	1.41	1
	SL	71.94	2.42	66.27	3.60	69.10	3.01	1
	MT [21]	79.80	1.70	69.78	2.81	74.79	2.25	2
	ICT [22]	80.58	1.58	72.62	2.72	76.59	2.15	2
	EM [23]	79.85	1.66	69.92	3.14	74.89	2.40	1
	UAMT [28]	79.62	1.67	71.98	2.55	75.78	2.11	8
	DAN [30]	80.47	1.56	74.62	2.74	77.55	2.15	2
20%	Ours	80.76	1.69	75.95	2.20	78.36	1.95	1
	SL	80.72	1.64	74.16	2.80	77.44	2.22	1
	MT [21]	81.09	1.54	76.30	2.30	78.70	1.92	2
	ICT [22]	81.86	1.53	77.42	2.32	79.64	1.92	2
	EM [23]	82.05	1.51	77.78	2.13	79.92	1.82	1
	UAMT [28]	81.38	1.60	77.47	2.30	79.43	1.95	8
	DAN [30]	81.68	1.53	78.09	2.27	79.88	1.90	2
	Ours	82.64	1.48	79.79	2.28	81.22	1.88	1

FT: the times of an input image passed the networks during one iteration (lower is better).

tation methods, including Mean Teacher (MT) [21], Interpolation Consistency Training (ICT) [22], Entropy Minimization (EM) [23], Uncertainty Aware Mean Teacher (UAMT) [28] and Deep Adversarial Network (DAN) [30]. Note that, for a fair comparison, we used a 3D UNet backbone network, and all of these implementations are online available [14]. Tab. 2 shows the quantitative comparison of these methods. It can be found that compared with the SL, all semi-supervised methods improve the segmentation performance by a large margin, as they can learn from the unannotated data by a regularization loss during the training, especially when just used 10% labeled data. The DAN [30] and EM [23] achieve the best results among existing methods respectively when using 10% and 20% labeled data, where the mean *DSC* was improved by 8.45% and 2.48% over the SL respectively. Our framework (URPC) achieves the best performance over the state-of-the-art semi-supervised methods when using 10% labeled data. After increasing the labeled data to 20%, our framework also outperforms the other methods in terms of DSC. These results show that our URPC has the capability to capture the rich information from the unlabeled data in addition to labeled data. What's more, the proposed URPC framework just needs to pass an input image once in an iteration, while most of the existing methods need twice or more, which increases the computational cost a lot. In Fig. 2, we visualize some 2D and 3D results of supervised and semi-supervised method when using 10% labeled data. The first, second and third rows show the GTVnx segmentation, GTVnd segmentation and 3D visualization respectively. Compared with supervised learning and DAN [30], our method has a higher overlap ratio with the ground truth and reduces the false negative in both slice level and volume level, especially in GTVnd segmentation (the second row). We further visualized the estimated uncertainty (\mathcal{D}_0 in Eq. 4) in Fig. 2 (d), it can be found that the uncertain region is mainly distributed near the boundary.

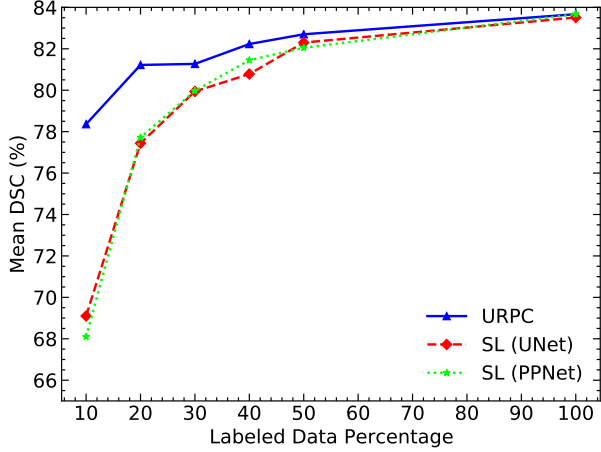


Fig. 3. The mean GTVnx and GTVnd segmentation performance of our semi-supervised approach with different ratio of annotated images. SL (UNet) and SL (PPNet) denote supervised learning from available annotated images using UNet and PPNet, respectively.

Impact of the different labeled data ratio. We also performed a study on the data utilization efficiency of the URPC compared against the SL (UNet) and SL (PPNet), where SL (UNet) and SL (PPNet) denote supervised learning from available annotated images using UNet and PPNet, respectively. Fig. 3 shows the evolution curve of mean *DSC* of GTVnx and GTVnd segmentation with the labeled data ratio increasing. It can be found that the URPC consistently performs better than the SL (UNet) and SL (PPNet) when using different ratios of labeled data, corroborating that the URPC has the capability to utilize the unlabeled data to bring performance gains. At the same time, the improvement margin of the proposed URPC over the partially supervised approaches become slight when more labeled images are available, which conforms to common sense [12, 15]. Although the labeled data ratio is very small, etc. 20%, the URPC also obtain a better segmentation than supervised learning methods with more labeled data (40% labeled data), indicating the promising potential of the proposed approach for further utilizing the abundant unlabeled data to develop high-performance segmentation models.

4 Discussion and Conclusion

In this work, we found that it is useful for semi-supervised learning to encourage the multi-scale outputs of PPNet to produce consistent predictions. We design a novel pyramid consistency loss to utilize the unlabeled data efficiently. Inspired by existing works [3, 25, 28, 31], we also use uncertainty maps to select reliable pixels for robust unsupervised learning. Compared with these methods, the advantage of our method as follows: (1) Thanks to the multiple predictions in PPNet, we can measure the uncertainty in a single forward pass by calculating the variance of these predictions, which

is much more efficient than the commonly used MC dropout that requires multiple forward passes; (2) Our method automatically selects reliable pixels rather than manually designing a threshold to cut off. In this work, we just apply the URPC for NPC GTV segmentation but it also can be used to segment other lesions and organs as it does not rely on any task-specific knowledge. Recently, some works, such as multi-head/decoder network and grouped convolution-based CNNs [24] can also produce multiple predictions and estimate the model uncertainty in a single forward pass. However, these methods are limited by the computational cost, as the grouped convolution-based CNN and multi-head/decoder network increase the model capacity and require more GPU memory in the same batch size. In addition, they are just designed to deal with interactive refinement and uncertainty estimation respectively and lack of evaluation in semi-supervised learning.

In this paper, we proposed a novel semi-supervised learning framework URPC for medical image segmentation. A pyramid prediction network is employed to learn from the unlabeled data by encouraging to produce consistent predictions at multiple scales. An uncertainty rectifying module is designed to improve the stability of learning from unlabeled images and further boost model performance. We applied the proposed method to the segmentation of GTVnx and GTVnd and the results demonstrated the effectiveness and generalization of URPC and also indicated the promising potential of our proposed approach for further clinical use. In the future, we will evaluate the framework on other segmentation tasks.

5 Acknowledgment

This work was supported by the National Natural Science Foundations of China [81771921, 61901084], and also by key research and development project of Sichuan province, China [20ZDYZF2817]. We thank M.D. Mengwen Wu and Yuanyuan Shen from the Sichuan Provincial People's Hospital for the data annotation and refinement.

References

1. Bai, W., Oktay, O., Sinclair, M., Suzuki, H., Rajchl, M., Tarroni, G., Glocker, B., King, A., Matthews, P.M., Rueckert, D.: Semi-supervised learning for network-based cardiac mr image segmentation. In: MICCAI. pp. 253–260. Springer (2017)
2. Bortsova, G., Dubost, F., Hogeweg, L., Katramados, I., de Bruijne, M.: Semi-supervised medical image segmentation via learning consistency under transformations. In: MICCAI. pp. 810–818. Springer (2019)
3. Cao, X., Chen, H., Li, Y., Peng, Y., Wang, S., Cheng, L.: Uncertainty aware temporal-ensembling model for semi-supervised abus mass segmentation. TMI (2020)
4. Chaitanya, K., Karani, N., Baumgartner, C.F., Becker, A., Donati, O., Konukoglu, E.: Semi-supervised and task-driven data augmentation. In: IPMI. pp. 29–41. Springer (2019)
5. Chen, W., Zheng, R., Baade, P.D., Zhang, S., Zeng, H., Bray, F., Jemal, A., Yu, X.Q., He, J.: Cancer statistics in china, 2015. CA: a cancer journal for clinicians 66(2), 115–132 (2016)
6. Çiçek, Ö., Abdulkadir, A., Lienkamp, S.S., Brox, T., Ronneberger, O.: 3d u-net: learning dense volumetric segmentation from sparse annotation. In: MICCAI. pp. 424–432. Springer (2016)

7. Cui, W., Liu, Y., Li, Y., Guo, M., Li, Y., Li, X., Wang, T., Zeng, X., Ye, C.: Semi-supervised brain lesion segmentation with an adapted mean teacher model. In: IPMI. pp. 554–565. Springer (2019)
8. Gal, Y., Ghahramani, Z.: Dropout as a bayesian approximation: Representing model uncertainty in deep learning. In: ICML. pp. 1050–1059 (2016)
9. Hang, W., Feng, W., Liang, S., Yu, L., Wang, Q., Choi, K.S., Qin, J.: Local and global structure-aware entropy regularized mean teacher model for 3d left atrium segmentation. In: MICCAI. pp. 562–571. Springer (2020)
10. Laine, S., Aila, T.: Temporal ensembling for semi-supervised learning. arXiv preprint arXiv:1610.02242 (2016)
11. Li, S., Zhang, C., He, X.: Shape-aware semi-supervised 3d semantic segmentation for medical images. In: MICCAI. pp. 552–561. Springer (2020)
12. Li, X., Yu, L., Chen, H., Fu, C.W., Xing, L., Heng, P.A.: Transformation-consistent self-ensembling model for semisupervised medical image segmentation. TNNLS (2020)
13. Lin, L., Dou, Q., Jin, Y.M., Zhou, G.Q., Tang, Y.Q., Chen, W.L., Su, B.A., Liu, F., Tao, C.J., Jiang, N., et al.: Deep learning for automated contouring of primary tumor volumes by mri for nasopharyngeal carcinoma. Radiology 291(3), 677–686 (2019)
14. Luo, X.: SSL4MIS. <https://github.com/HiLab-git/SSL4MIS> (2020)
15. Luo, X., Chen, J., Song, T., Chen, Y., Wang, G., Zhang, S.: Semi-supervised medical image segmentation through dual-task consistency. arXiv preprint arXiv:2009.04448 (2020)
16. Ma, J., Nie, Z., Wang, C., Dong, G., Zhu, Q., He, J., Gui, L., Yang, X.: Active contour regularized semi-supervised learning for covid-19 ct infection segmentation with limited annotations. Physics in Medicine & Biology (2020)
17. Nie, D., Gao, Y., Wang, L., Shen, D.: Asdnet: Attention based semi-supervised deep networks for medical image segmentation. In: MICCAI. pp. 370–378. Springer (2018)
18. Paszke, A., Gross, S., Massa, F., Lerer, A., Bradbury, J., Chanan, G., Killeen, T., Lin, Z., Gimelshein, N., Antiga, L., et al.: Pytorch: An imperative style, high-performance deep learning library. In: NeurIPS. pp. 8026–8037 (2019)
19. Peng, J., Pedersoli, M., Desrosiers, C.: Mutual information deep regularization for semi-supervised segmentation. In: MIDL. pp. 601–613. PMLR (2020)
20. Qiao, S., Shen, W., Zhang, Z., Wang, B., Yuille, A.: Deep co-training for semi-supervised image recognition. In: ECCV. pp. 135–152 (2018)
21. Tarvainen, A., Valpola, H.: Mean teachers are better role models: Weight-averaged consistency targets improve semi-supervised deep learning results. In: NeurIPS. pp. 1195–1204 (2017)
22. Verma, V., Lamb, A., Kannala, J., Bengio, Y., Lopez-Paz, D.: Interpolation consistency training for semi-supervised learning. In: IJCAI. pp. 3635–3641 (2019)
23. Vu, T.H., Jain, H., Bucher, M., Cord, M., Pérez, P.: Advent: Adversarial entropy minimization for domain adaptation in semantic segmentation. In: CVPR. pp. 2517–2526 (2019)
24. Wang, G., Aertsen, M., Deprest, J., Ourselin, S., Vercauteren, T., Zhang, S.: Uncertainty-guided efficient interactive refinement of fetal brain segmentation from stacks of mri slices. In: MICCAI. pp. 279–288. Springer (2020)
25. Wang, G., Li, W., Aertsen, M., Deprest, J., Ourselin, S., Vercauteren, T.: Aleatoric uncertainty estimation with test-time augmentation for medical image segmentation with convolutional neural networks. Neurocomputing 338, 34–45 (2019)
26. Wang, Y., Zhang, Y., Tian, J., Zhong, C., Shi, Z., Zhang, Y., He, Z.: Double-uncertainty weighted method for semi-supervised learning. In: MICCAI. pp. 542–551. Springer (2020)
27. Xia, Y., Liu, F., Yang, D., Cai, J., Yu, L., Zhu, Z., Xu, D., Yuille, A., Roth, H.: 3d semi-supervised learning with uncertainty-aware multi-view co-training. In: WACV. pp. 3646–3655 (2020)

28. Yu, L., Wang, S., Li, X., Fu, C.W., Heng, P.A.: Uncertainty-aware self-ensembling model for semi-supervised 3d left atrium segmentation. In: MICCAI. pp. 605–613. Springer (2019)
29. Yushkevich, P.A., Piven, J., Hazlett, H.C., Smith, R.G., Ho, S., Gee, J.C., Gerig, G.: User-guided 3d active contour segmentation of anatomical structures: significantly improved efficiency and reliability. *Neuroimage* 31(3), 1116–1128 (2006)
30. Zhang, Y., Yang, L., Chen, J., Fredericksen, M., Hughes, D.P., Chen, D.Z.: Deep adversarial networks for biomedical image segmentation utilizing unannotated images. In: International Conference on Medical Image Computing and Computer-Assisted Intervention. pp. 408–416. Springer (2017)
31. Zheng, Z., Yang, Y.: Rectifying pseudo label learning via uncertainty estimation for domain adaptive semantic segmentation. *arXiv preprint arXiv:2003.03773* (2020)
32. Zhou, Y., Wang, Y., Tang, P., Bai, S., Shen, W., Fishman, E., Yuille, A.: Semi-supervised 3d abdominal multi-organ segmentation via deep multi-planar co-training. In: WACV. pp. 121–140. IEEE (2019)